nature nanotechnology

ARTICLES

https://doi.org/10.1038/s41565-020-0723-4



# Engineering synthetic breath biomarkers for respiratory disease

Leslie W. Chan[1], Melodi N. Anahtar[1,2], Ta-Hsuan Ong[3], Kelsey E. Hern[2], Roderick R. Kunz[3] and Sangeeta N. Bhatia[1,2,4,5,6,7] ✉

**Human breath contains many volatile metabolites. However, few breath tests are currently used in the clinic to monitor disease due to bottlenecks in biomarker identification. Here we engineered breath biomarkers for respiratory disease by local delivery of protease-sensing nanoparticles to the lungs. The nanosensors shed volatile reporters upon cleavage by neutrophil elastase, an inflammation-associated protease with elevated activity in lung diseases such as bacterial infection and alpha-1 antitrypsin deficiency. After intrapulmonary delivery into mouse models with acute lung inflammation, the volatile reporters are released and expelled in breath at levels detectable by mass spectrometry. These breath signals can identify diseased mice with high sensitivity as early as 10 min after nanosensor administration. Using these nanosensors, we performed serial breath tests to monitor dynamic changes in neutrophil elastase activity during lung infection and to assess the efficacy of a protease inhibitor therapy targeting neutrophil elastase for the treatment of alpha-1 antitrypsin deficiency.**

Clinical detection and monitoring of disease largely rely on blood and urine assays. Alternatively, breath is a practical and potentially informative clinical analyte because it can be sampled non-invasively and contains hundreds of trace volatile organic compounds (VOCs) that are produced in the body as metabolites or from environmental exposure[1–3]. However, harnessing breath volatiles for clinical diagnostics has been a challenging and slow process. Low and variable VOC concentrations (ppt to low ppm) and confounding VOCs from the diet and the environment have hindered the identification of robust breath biomarkers[4]. Furthermore, standard biomarker identification methods using gas chromatography–mass spectrometry suffer from statistical and technical challenges, such as false correlations due to overfitting models to high dimensional datasets and a trade-off between the number of VOCs analysed and precision in VOC identification and quantification[5].

One approach to overcome these challenges is the in vivo administration of exogenous agents that are metabolized into volatile products by disease-specific molecular processes. Examples include the $^{13}$C-urea breath test for *Helicobacter pylori* detection and the $^{13}$C-methacetin breath test for liver fibrosis, in which isotope-labelled small molecules are ingested and selectively metabolized by urease secreted by *H. pylori* and hepatic cytochrome P450, respectively, into $^{13}CO_2$ (refs. [6,7]). Similarly, small intestinal bacterial overgrowth is diagnosed by tracking peaks in breath hydrogen levels that correspond to bacterial fermentation after disaccharide ingestion[8]. These clinical tests and others in development[5,9,10] leverage known enzyme biology to produce breath readouts, and in the case of $^{13}$C breath tests, produce a volatile that is not naturally found in the body, thereby maximizing signal-to-noise ratio (SNR). The application of exogenous agents in clinical breath tests has been predominantly used to diagnose gastrointestinal and liver diseases and is more recently being investigated for respiratory disease[11,12]. As the direct source of breath, the lungs are particularly suited for interrogation using enzymatic activity-based breath tests. Current diagnostic tools for respiratory illness include chest X-rays, spirometry, sputum cytology and/or microbiological tests, which can have poor sensitivity, specificity or, in the case of microbiological testing, long testing times that delay appropriate treatment[13–15]. Breath tests may enable rapid disease detection and monitoring and, in combination with other current tests, provide further actionable information at the point of care.

Here, we report a class of nanoscale agents, volatile-releasing activity-based nanosensors (vABNs), engineered for intrapulmonary delivery and subsequent protease-driven release of volatile reporters. Proteases are implicated in the pathology of numerous lung diseases, including cancer, fibrosis, chronic obstructive pulmonary disease and respiratory infections[16,17]. To leverage protease activity for disease detection, we have previously engineered activity-based nanosensors (ABNs) consisting of mass- or ligand-encoded reporters tethered to long-circulating nanoparticle scaffolds via protease-cleavable peptide linkers[18]. After intravenous administration, peptide linkers are cleaved by target proteases in diseased tissues, releasing reporters into circulation for subsequent renal clearance and production of a urinary readout. Similarly, after intrapulmonary delivery, vABNs are exposed to proteases in the diseased lung that cleave surface-conjugated peptides and release volatile reporters into the alveolar space for exhalation (Fig. 1). The use of bio-orthogonal volatile reporters allows us to easily distinguish our reporters from the complex biological matrix of endogenous VOCs in the breath. We have previously demonstrated the feasibility of protease-driven urinary readouts for disease detection and stratification, and treatment monitoring in preclinical models of cancer, liver fibrosis, thrombosis and

[1]Koch Institute for Integrative Cancer Research, Massachusetts Institute of Technology, Cambridge, MA, USA. [2]Harvard–MIT Division of Health Sciences and Technology, Institute for Medical Engineering and Science, Massachusetts Institute of Technology, Cambridge, MA, USA. [3]Biological and Chemical Technologies Group, Massachusetts Institute of Technology Lincoln Laboratory, Lexington, MA, USA. [4]Department of Electrical Engineering and Computer Science, Massachusetts Institute of Technology, Cambridge, MA, USA. [5]Department of Medicine, Brigham and Women's Hospital, Harvard Medical School, Boston, MA, USA. [6]Broad Institute, Massachusetts Institute of Technology and Harvard, Cambridge, MA, USA. [7]Howard Hughes Medical Institute, Cambridge, MA, USA. ✉e-mail: sbhatia@mit.edu

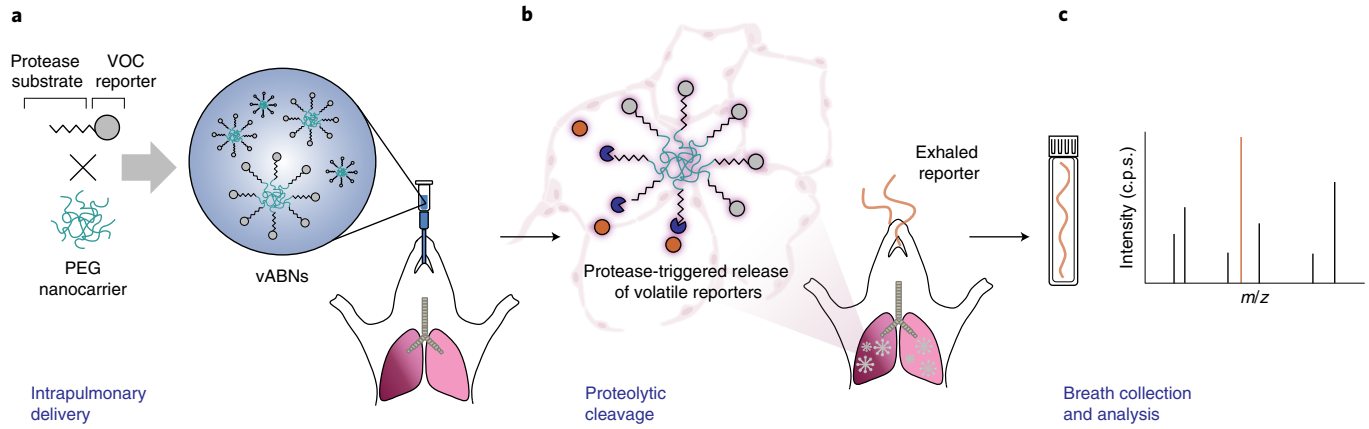


**Fig. 1 | Schematic of the approach. a**, VOC-modified peptide substrates are formulated into vABNs by conjugation onto an eight-arm PEG nanocarrier and delivered into the lungs via intratracheal instillation. **b**, When attached to the vABN, VOC reporters are in an undetectable, non-volatile state (grey). Extracellular proteases produced during respiratory disease cleave surface-conjugated peptide substrates, thereby releasing VOC reporters. Upon release from vABNs, reporters recover their characteristic mass and volatility (orange) and are then exhaled. **c**, Breath is collected into a receptacle (for example, an evacuated glass vial), and VOC reporter concentration is quantified using mass spectrometry.

infection[18–22]. In this work, the serine protease neutrophil elastase (NE) was selected as the target protease. During inflammation, NE is released by neutrophils to kill microbial pathogens and regulate leucocyte recruitment[23]. Due to its elastin-rich composition, the lung is also susceptible to damage by elastases. Therefore, NE plays a notable role in numerous lung diseases, including pulmonary infection, which is the most common risk factor for acute lung injury[24], and alpha-1 antitrypsin deficiency (AATD), in which damaging NE activity is elevated due to the absence of its inhibitor[25]. Here, we engineer the vABN platform and demonstrate the ability to track pulmonary NE activity through breath analysis within ten minutes of vABN delivery. Using vABN breath tests, we non-invasively monitor NE activity in lung infection and AATD, and NE inhibition during AATD treatment.

## Development of vABNs

To engineer vABNs, we chemically modified peptide substrates to release a volatile reporter upon cleavage. We selected an optimized fluorogenic tetrapeptide substrate with the sequence Ac-Nle(O-Bzl)-Met(O)$_2$-Oic-Abu-ACC (ACC, fluorophore reporter 7-amino-4-carbamoylmethylcoumarin) due to its selectivity for both human and mouse NE, catalytic efficiency and cleavage site between the C-terminal residue (Abu) and the fluorophore reporter[26,27]. We hypothesized that an amine-containing VOC could be attached via an amide bond to the peptide C-terminus in place of the fluorophore reporter while maintaining substrate susceptibility to NE. Furthermore, we predicted this attachment chemistry would allow the released VOC to recover its characteristic mass and volatility to undergo phase transition for detection as a gas (Fig. 2a). Hydrofluoroamines (HFAs) with the chemical formula $CF_3(CF_2)_xCH_2NH_2$ were selected as bio-orthogonal VOC reporters due to their high volatility. In this work, HFA reporters will be referred to as HFA$x$, where $x$ is the $CF_2$ chain length (chemical names and CAS registry numbers provided in Supplementary Table 1). To test our hypothesis, we synthesized an HFA1-modified NE peptide substrate and used mass spectrometry to characterize the substrate and reporter behaviour in the presence of active NE (Fig. 2b). Before NE addition, no HFA1 was detected in the headspace of vials containing the solubilized, intact substrate. After NE addition, the substrate was cleaved between the Abu residue and HFA1 reporter, and freed reporters partitioned rapidly from solution into the vial headspace.

HFA1-releasing substrate was subsequently formulated into vABNs for intrapulmonary delivery. Low-molecular-weight macromolecules readily escape the lungs by diffusion across the thin alveolar walls into blood circulation[28]. To prolong retention in the lungs, substrates were conjugated to 40 kDa eight-arm poly(ethylene glycol) (PEG) nanocarriers, which distribute throughout the lungs (Supplementary Fig. 1) and have a half-life of several days after intratracheal instillation[22,29]. The average diameter of completed vABNs was $8.7 \pm 2.1$ nm (Fig. 2c). vABNs demonstrated linear, dose-dependent reporter release in response to human and mouse NE, down to picomolar concentrations in vitro (Fig. 2d and Supplementary Fig. 2a). Negligible reporter release was triggered by other proteases that might be present in the lungs, both in optimized buffer conditions (Fig. 2e) and in simulated lung fluid[30,31] (Supplementary Fig. 3).

## In silico prediction of breath signal after vABN delivery

Having established methods for vABN synthesis, we built a physiologically based pharmacokinetic (PBPK) model to investigate and optimize parameters important for a breath signal. PBPK models for the respiratory tract are well-established in the toxicology field[32–36]. By incorporating cleavage kinetics, we developed a PBPK model that is governed by a set of differential equations representing the sequence of events leading to a breath readout following vABN delivery (Fig. 3a and Supplementary Information). These events include (i) vABN accumulation in diseased lung tissue, (ii) peptide cleavage by proteases/reporter release, (iii) partitioning of freed reporters from lung tissue to the respiratory lumen, (iv) exhalation of freed reporters and (v) breath analysis. The model output (breath signal over time) resembles washout curves from existing breath tests in which breath signal rapidly rises due to the metabolic breakdown of the substrate followed by a peak and decline as the administered dose is depleted[7,37]. We hypothesized that protease abundance, vABN dose, cleavage kinetics and partitioning of freed reporters into air (over tissue or blood) were key parameters influencing the magnitude of the breath signal generated over time. Protease abundance and vABN dose were varied in the model to determine their effect on detection sensitivity and are further described in the Supplementary Information (Supplementary Fig. 4a,b). Of note, the model predicted that micromolar substrate doses produce ppb-range reporter concentrations in breath, which are well above the mass spectrometer ppt detection limit.

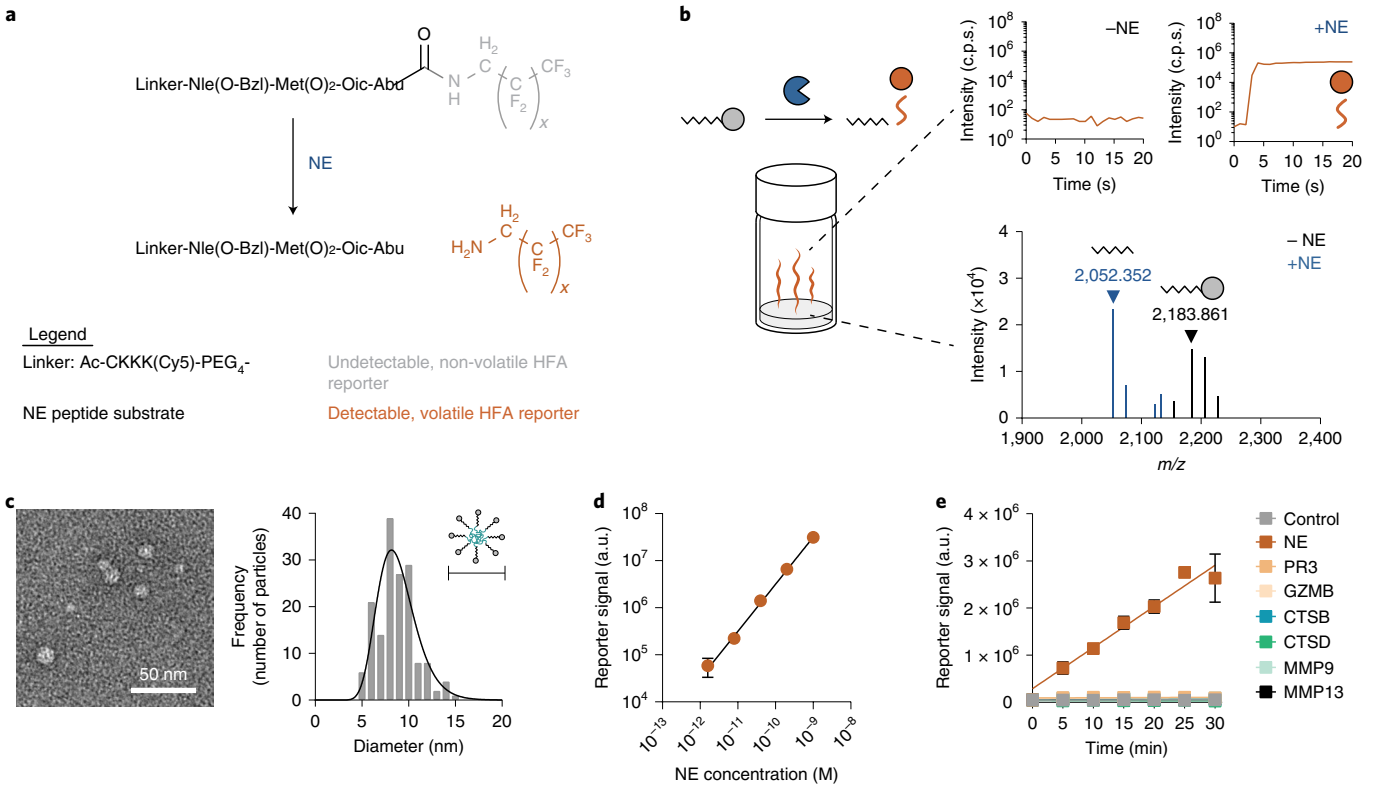


**Fig. 2 | vABNs are activated by human NE and release volatile reporters detectable by mass spectrometry. a**, Chemical structure of HFA-modified NE peptide substrates. HFA reporters are attached at the C-terminus via an amide bond. A cysteine is included in the hydrophilic linker at the N-terminus for conjugation to a nanoparticle carrier. **b**, Matrix-assisted laser desorption/ionization time-of-flight (MALDI-TOF) mass spectrum confirming HFA1 release after substrate cleavage by purified human NE (bottom) and mass spectra from real-time vapour analysis confirming partitioning of the freed reporter into the reaction headspace (top). **c**, Transmission electron microscopy (TEM) image of nanoformulated substrates (that is, vABNs) for particle sizing. The histogram shows particle size distribution ($n=160$ particles). The solid line represents the Gaussian fit of the size distribution. **d**, In vitro HFA1 release from vABNs as a function of NE concentration. **e**, In vitro HFA1 release from vABNs triggered by NE and other proteases associated with respiratory disease to assess sensor specificity. (**d**,**e**, mean ± s.d., $n=3$ independent measurements). All cleavage experiments were completed independently twice with similar results.

Furthermore, the predicted breath signals peak within 15 min of vABN delivery and return to the baseline by 2 h.

While protease concentrations are inherent to the disease state, and vABN dosing is easily adjusted, cleavage rate and reporter partitioning are governed by vABN composition. vABNs can be synthesized with HFA reporters of varying size, which partition differently into the three compartments—lung tissue (t), blood (b) and respiratory lumen/air (a)—after release. Partition coefficients ($H_{t:a}$ and $H_{b:a}$) and their quotient ($H_{t:b}$) define the ratio of reporters between two compartments at equilibrium. As $H_{b:a}$ increases in favour of the blood compartment, $H_{t:b}$ decreases and more reporter is cleared from lung tissue into blood and unavailable for partitioning into lumen (Supplementary Fig. 4c,d). Therefore, reporters with lower $H_{b:a}$ should provide a greater breath signal. We determined

**Fig. 3 | In silico and in vivo investigation of parameters contributing to the breath signal facilitate vABN optimization. a**, Multicompartment PBPK model built to predict volatile reporter concentrations in breath following intrapulmonary vABN delivery (*C*, concentration; *k*, rate constant; *H*, partition coefficient of the free reporter in tissue (t), blood (b), or the respiratory lumen/air (a); $Q_m$, flow rate). The model consists of differential equations representing the following: diffusion of nanoparticles (NP), or vABNs, from the respiratory lumen into the diseased lung tissue ($k^{NP}_{tissue}$), generation of freed reporters from NE cleavage of vABNs ($k^{NE}_{cat}$) and non-specific cleavage by other pulmonary proteases (NS) in the tissue compartment ($k^{NS}_{cat}$), partitioning of freed reporters from the tissue into the respiratory lumen ($k^{reporter}_{tissue}$, $H_{t:a}$) and subsequent exhalation in breath ($Q_m$), and the alternative route of reporter clearance from the lungs by diffusion from tissue into blood ($k^{reporter}_{clear}$, $H_{t:b}$). The model was used to investigate the effects of reporter size on breath signal generated by NE-sensing vABNs during lung infection. Parameters that change with reporter size are $H_{t:b}$ and the catalytic efficiency of vABN cleavage by NE ($k_{cat}/K_m$). **b**–**d**, Empirical values for both parameters were determined for a vABN panel containing the candidate reporters (HFA1, HFA3, HFA5 and HFA7; Table 1) and used in the model to predict the effect of each parameter in isolation (**b**,**c**) and their combined effects (**d**). Arrows indicate direction of increasing parameter values. Predicted breath signal for HFA7 is not included in **b** due to difficulty in vapourizing HFA7 for determination of its partition coefficient. For **d**, $H_{t:b}$ for HFA7 is assumed to be the same as that of HFA5. **e**, Schematic for characterization of vABN activity in a mouse model of acute lung infection. Immunofluorescence images show NE (green) in healthy lungs (top left) versus lungs infected with *P. aeruginosa* (top right), and co-localization of vABNs (magenta) with extracellular NE (green, bottom left) and intracellular vABN uptake (bottom right). DAPI staining is used for cell nuclei. White arrows indicate vABNs of interest. Immunofluorescence staining was completed independently twice with similar results. **f**, Breath signal after intrapulmonary delivery of HFA1-releasing vABNs in healthy controls and lung infection mouse models. Two concentrations were tested, 10 and 100 μM vABN by peptide concentration (mean ± s.d., $n=3$ or 4 mice per group). Area-under-the-curve analysis showed that the total reporters exhaled scaled with dose (46.1 and 398 pmol HFA1 for 10 and 100 μM, respectively). **g**, Breath signal after delivery of 10 μM vABNs containing HFA1, HFA3, HFA5 or HFA7 reporters (mean ± s.d., $n=3$ or 4 mice per group). Breath experiments were completed independently twice with similar results.

the partition coefficients for candidate reporters (HFA1, HFA3 and HFA5; Table 1) and, using the model, predicted that HFA3 and HFA5 would produce the greatest breath signal if partitioning were the only essential parameter (Fig. 3b). However, we hypothesized that the benefits of partitioning might be offset by changes to cleavage rates upon exchanging HFA1 for larger, bulkier HFA reporters that might

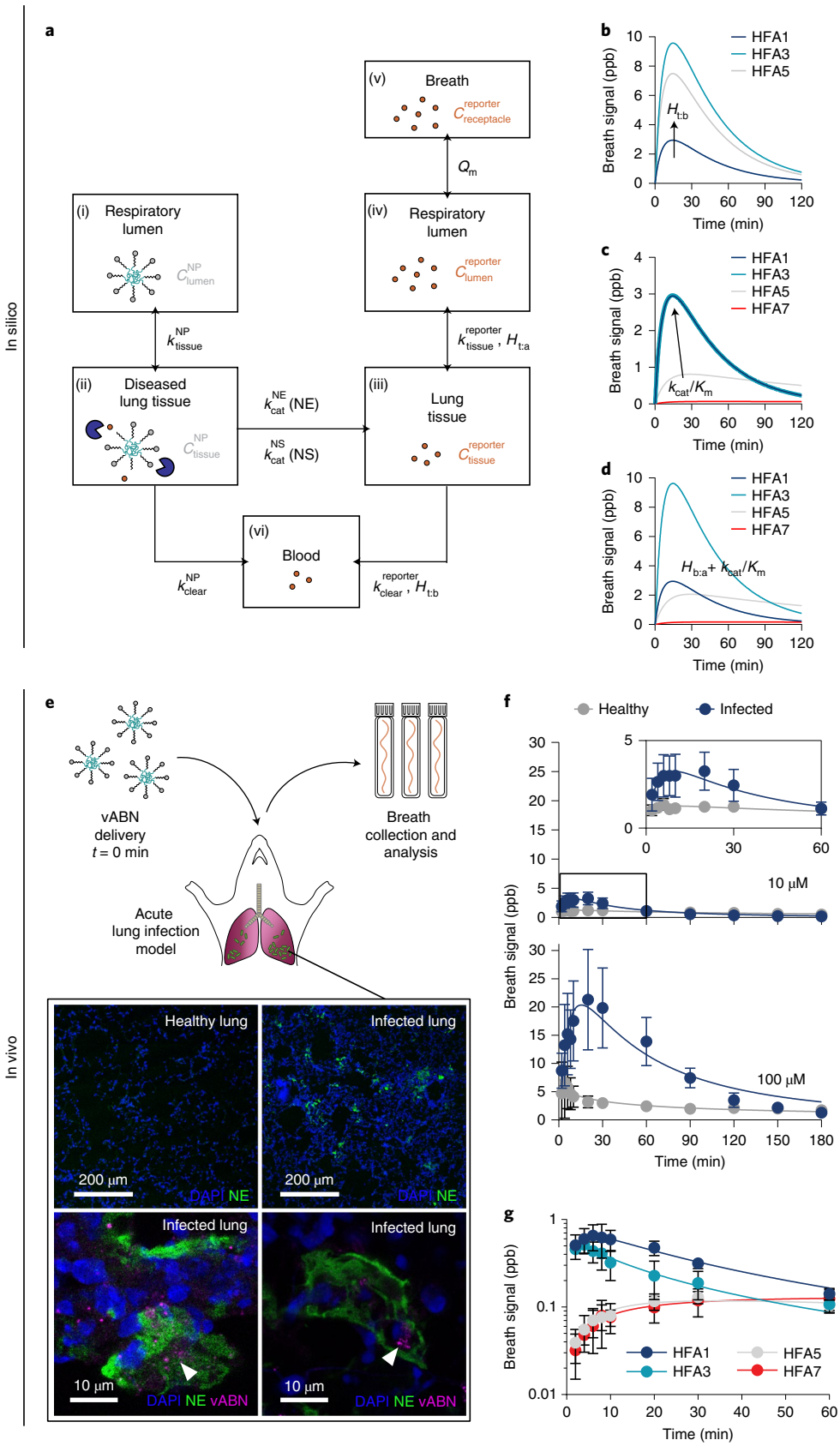

**Table 1 | Reporter partition coefficients and cleavage kinetic constants for vABNs**

| Reporter | MW | $H_{t:a}$ | $H_{b:a}$ | $H_{t:b}$ | $k_{cat}$, $s^{-1}$ | $K_m$, μM | $k_{cat}/K_m$, $M^{-1}s^{-1}$ ($\times 10^5$) |
|---|---|---|---|---|---|---|---|
| HFA1 | 149.1 | 57.64 | 65.16 | 0.88 | 3.10 (±1.15) | 10.91 (±1.35) | 2.79 (±0.75) |
| HFA3 | 249.1 | 137.24 | 20.06 | 6.84 | 3.40 (±0.55) | 11.98 (±0.68) | 2.83 (±0.39) |
| HFA5 | 349.1 | 58.89 | 25.63 | 2.30 | 2.78 (±2.64) | 66.78 (±42.52) | 0.51 (±0.33) |
| HFA7 | 449.1 | n.a. | n.a. | n.a. | 0.07 (±0.02) | 22.34 (±1.84) | 0.03 (±0.01) |

Catalytic rate constants and Michaelis–Menten constants shown represent the mean ± s.d. ($n = 3$ independent measurements). Experiments to determine partition coefficients and cleavage kinetic constants were completed independently twice with similar results. n.a., not applicable.

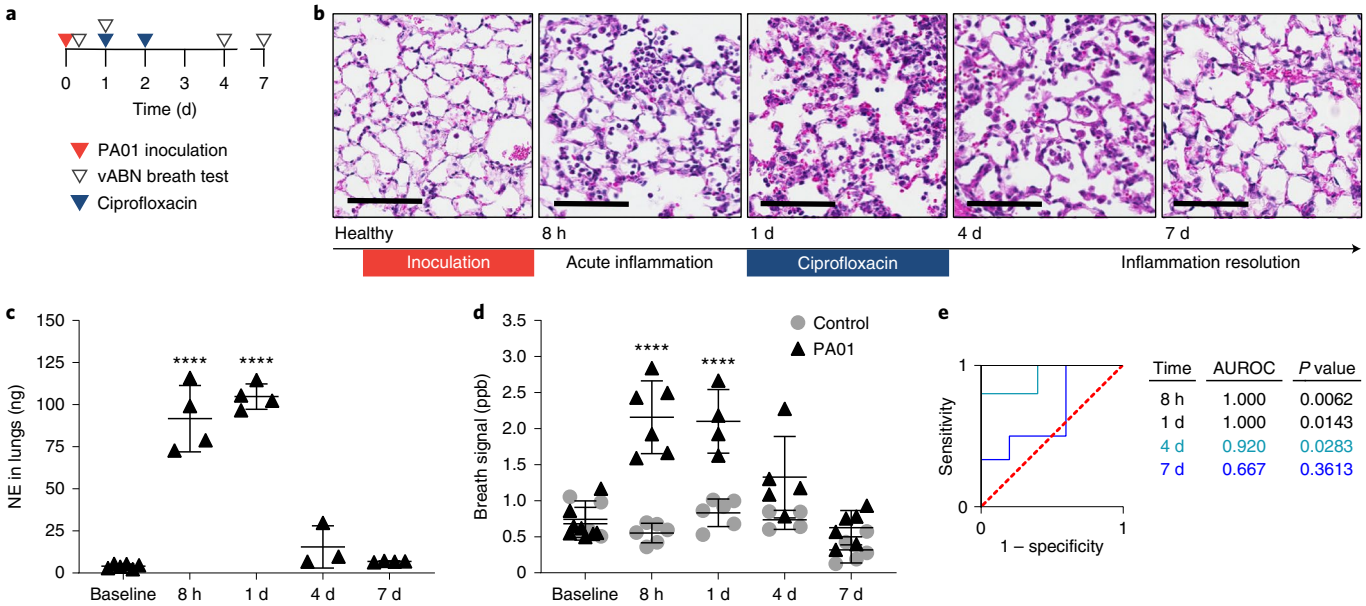


**Fig. 4 | Serial vABN breath tests enable monitoring of pulmonary NE activity during lung infection. a**, Experimental timeline for monitoring pulmonary NE activity before and after antibiotic treatment in lung infection mouse models. Each vABN breath test consists of delivery of 10 μM vABN, breath collection 10 min after vABN delivery and breath sample analysis by mass spectrometry. **b**, H&E-stained lung tissue sections showing the influx and recession of neutrophils after infection and antibiotic treatment (scale bar, 100 μm, $n = 3$ mice per time point). **c**, NE protein levels measured from lung homogenates (mean ± s.d., $n = 3$, 4 or 6 mice per group). **d**, Corresponding breath signal at each experimental time point (mean ± s.d., $n = 4$, 5, 6 or 8 mice per group). **e**, ROC curves showing the ability of the breath signal to distinguish PA01-inoculated mice from healthy controls over the course of infection. An AUROC of 1.0 indicates perfect distinction, while an AUROC of 0.5 indicates random classification (represented by the dashed red line). Distinction between control and PA01-inoculated groups diminishes as inflammation resolves, as evidenced by decreasing AUROC values with time ($n = 4$, 5, 6 or 8 mice per group as in **d**). **c**,**d**, One-way analysis of variance (ANOVA) with Tukey's multiple comparisons test, $^{****}P < 0.0001$. All experiments were completed independently twice with similar results.

adversely affect protease–substrate interactions. To test this hypothesis, we synthesized a vABN panel containing the candidate reporters, and the catalytic efficiency of substrate cleavage ($k_{cat}/K_m$, where $k_{cat}$ is the catalytic rate constant and $K_m$ is the Michaelis–Menten constant) was determined empirically to be used in the PBPK model (Table 1). The catalytic efficiency of HFA1-containing vABNs fell in between that of the parent, commercial substrate and the optimized peptide substrate ($10^3$–$10^7$ $M^{-1}s^{-1}$)[26]. Reduced catalytic efficiency is likely due to nanoparticle sterics[19] and/or the modification of the P1′ position[38]. Catalytic efficiency is further reduced by up to two orders of magnitude when HFA1 is replaced by larger reporters. Thus, when solely considering this parameter, the predicted breath signal was greater for vABNs containing smaller HFAs (Fig. 3c). With the exception of HFA3, which has all-around favourable parameter values, rankings of candidate reporters based on the combined effects of cleavage kinetics and partitioning were nonintuitive. Using the PBPK model, we were able to identify HFA1 and HFA3 as our top candidate reporters based on maximum breath signal (Fig. 3d).

Using the PBPK model, we explored a final parameter, $k^{NP}_{tissue}$, that describes the nanoparticle transport rate from the lumen into the lung tissue (that is, the compartment containing NE). $k^{NP}_{tissue}$ is a function of particle size, which is determined by the choice of carrier. As particle size increases and approaches micrometre-scale diameter, $k^{NP}_{tissue}$decreases and predicted breath signal approaches sub-ppb levels due to poor NE accessibility (Supplementary Fig. 5a). With validation from the PBPK model, we moved forward with our nanoscale sensors.

## In vivo investigation of vABN-derived breath signal

We moved to a mouse model of acute lung infection[20] to verify the feasibility of a protease-driven breath signal (Fig. 3e). In this model, NE protein levels in the lungs are elevated ~20-fold by 12 h after intratracheal instillation of Gram-negative *Pseudomonas aeruginosa* (Supplementary Fig. 6). After intrapulmonary delivery of 10 and 100 μM vABNs in infection models, breath collected over 1–3 h contained dose-dependent, ppb-range reporter concentrations (Fig. 3f).

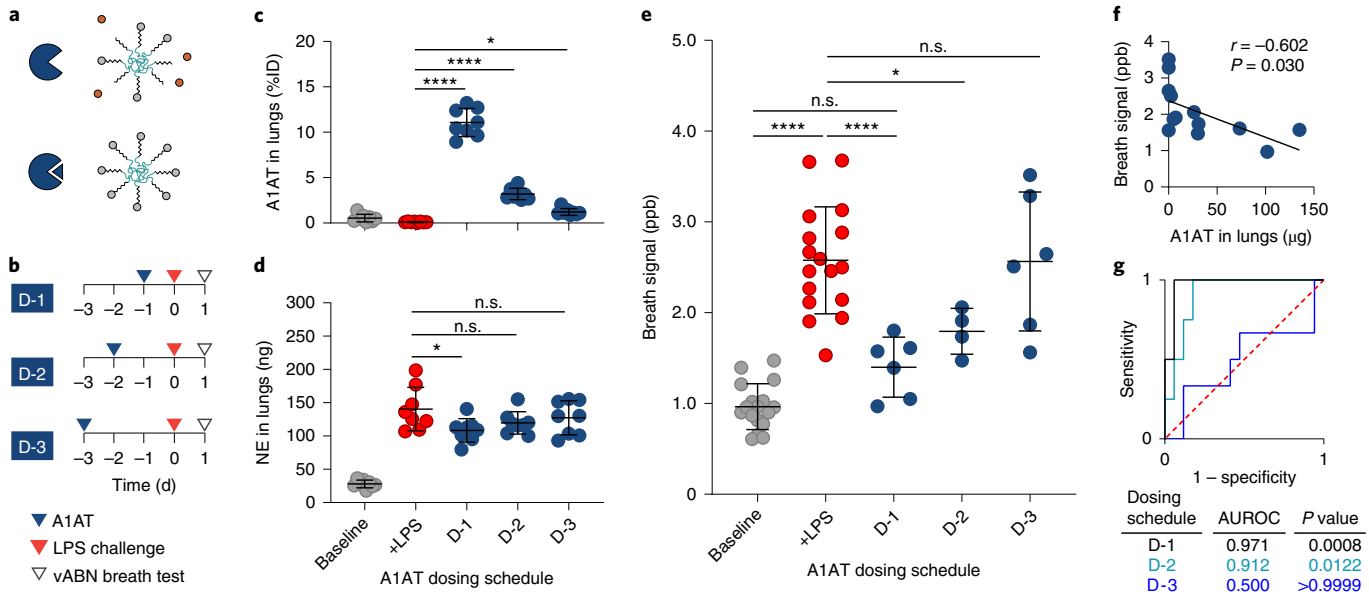


**Fig. 5 | vABN-derived breath signal can be used to assess duration of NE inhibition following A1AT treatment. a**, Schematic showing vABN reporter release triggered by active NE (top) and attenuated reporter release due to NE inhibition by A1AT (bottom). **b**, A1AT dosing schedules to assess the duration of NE inhibition after a single prophylactic dose of A1AT. **c**, Percent of the initial A1AT dose (%ID) remaining in the lungs by the day of the breath test (mean ± s.d., $n = 8$ mice per group, one-way ANOVA with Tukey's multiple comparisons test, $^{*}P = 0.0259$, $^{****}P < 0.0001$). **d**, NE in the lungs on the day of the breath test (mean ± s.d., $n = 8$ mice per group, one-way ANOVA with Tukey's multiple comparisons test, $^{*}P = 0.0188$, n.s. = not significant where $P = 0.1868$ for +LPS versus D-2 comparison and $P = 0.5697$ for +LPS versus D-3 comparison). **e**, Breath signal 24 h after LPS is administered in the lungs of untreated mice (red) and A1AT-pretreated mice (blue; mean ± s.d., $n = 4$, 6 or 17 mice per group, one-way ANOVA with Tukey's multiple comparisons test, $^{*}P = 0.0244$, $^{****}P < 0.0001$, n.s. = not significant where $P = 0.3221$ for baseline versus D-1 comparison and $P > 0.9999$ for +LPS versus D-3 comparison). **f**, Dot plot showing correlation between breath signal and A1AT in the lungs for D-1, D-2 and D-3 cohorts shown in **e**. Pearson's correlation coefficient, $r$, was calculated assuming a Gaussian distribution. The $P$ value was determined using a two-tailed $t$-test ($n = 13$ mice). **g**, ROC curves showing the ability of the breath signal from **e** to distinguish between untreated, LPS-challenged mice ($n = 17$ mice) and mice given a 1 mg dose of A1AT 1, 2 or 3 days before the LPS challenge ($n = 4$ or 6 mice per group). Distinction between untreated and treated mice diminishes with increasing time between A1AT dosing and the LPS challenge. By day 3 after a single 1 mg dose of A1AT, no protection against NE activity is observed.

The maximum breath signal in infected mice was observed 10–20 min after vABN administration, was elevated relative to that of healthy controls and returned to control levels within 1–3 h (Fig. 3f). These results are consistent with PBPK model predictions. Experimental controls for breath collection and analysis methods[39,40] confirmed that the vast majority of reporter signal is derived from breath rather than other sources such as urine (Supplementary Fig. 7), and that no background signal is present in the absence of vABN administration (Supplementary Fig. 8).

We next sought to validate model predictions for optimal vABN composition. Breath analysis after administration of 10 μM vABNs containing HFA1, HFA3, HFA5 and HFA7 reporters revealed that vABNs with HFA1 and HFA3 produced the highest breath signal and most rapid signal kinetics (Fig. 3g). We next investigated SNR by comparing diseased versus healthy breath signals. HFA1-releasing vABNs produced higher average SNR than HFA3-releasing vABNs at the 10 μM dose (Supplementary Fig. 9). Furthermore, HFA1-containing vABNs were stable in simulated lung fluid, while HFA3-containing vABNs readily precipitated (Supplementary Fig. 10), which may account for the differences between predicted and observed breath signals. We observed no acute toxicity 24 h after in vivo administration of HFA1-containing vABNs for concentrations up to 100 μM (Supplementary Fig. 11). Given their SNR, stability in a simulated lung fluid and limited toxicity, we moved forward with HFA1-containing vABNs for subsequent experiments.

We next verified that breath signal was specifically driven by NE activity. Sivelestat, a small molecule inhibitor of human and mouse NE (ref. [41]), prevents vABN cleavage in vitro (Supplementary Fig. 2b). When administered in infected mice, the inhibitor attenuated the average breath signal by ~75%, demonstrating the role of NE activity in driving reporter release in vivo (Supplementary Fig. 12). Immunohistological staining of infected lung tissue sections and confocal imaging confirmed vABN co-localization with extracellular NE (Fig. 3e). Though intracellular vABN uptake was also observed in lung tissue sections, rapid breath signal kinetics suggests that reporter release is predominantly triggered by extracellular NE activity. Furthermore, peptide substrate delivery on a nanocarrier resulted in a prolonged, elevated breath signal in infected mice compared to delivery of free peptide (Supplementary Fig. 5b,c), demonstrating that the nanocarrier increases peptide accessibility to NE. Taken together, this data demonstrates the feasibility of using vABNs to generate a rapid breath readout for pulmonary protease activity.

## Respiratory disease monitoring through vABN breath tests

Disease progression and resolution are marked by changes in protease activity[42]. Therefore, tools that sense protease activity can be leveraged to monitor disease during treatment. Using serial vABN breath tests, we monitored changes to NE activity during the progression and resolution of lung infection. To model disease dynamics, mice were inoculated with *P. aeruginosa* to trigger acute inflammation and neutrophil recruitment to the lungs and then treated 1–2 d post-inoculation with an antibiotic, ciprofloxacin, to kill bacteria and allow neutrophil clearance (Fig. 4a). Lung tissue sections stained with hematoxylin and eosin (H&E) showed increasing neutrophil infiltration at 8 h and 1 d and diminishing neutrophil presence at 4 d and 7 d (Fig. 4b). A corresponding rise and fall of NE

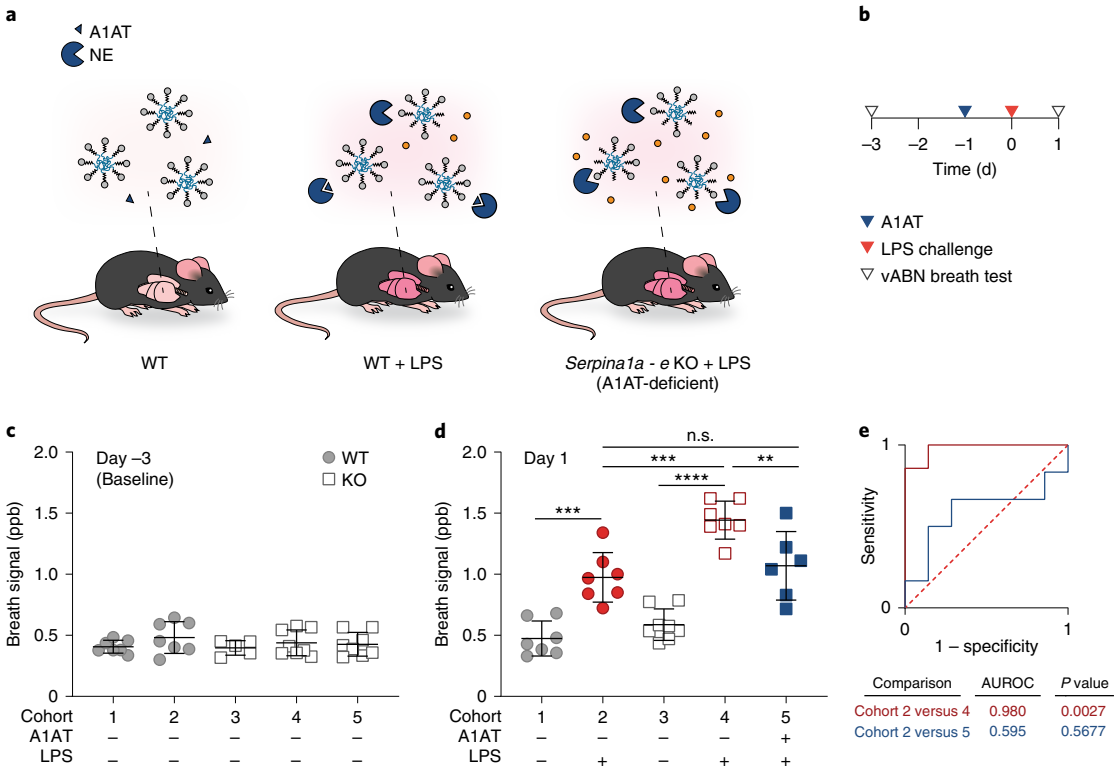


**Fig. 6 | vABN breath tests can resolve normal and pathologic NE activity for assessment of A1AT augmentation therapies. a**, Schematic showing expected trends for vABN cleavage in WT C57BL/6 and C57BL/6 *Serpina1a* - *e* KO mice. **b**, Experimental timeline for comparison of breath signal in WT and KO mice before and during inflammation. A 1 mg dose of A1AT is administered 24 h before the LPS challenge only in the treated group (cohort 5 in subsequent panels). **c**, Baseline breath signal measured on day −3 (mean ± s.d., $n = 7$ or 8 mice per group). **d**, Breath signal measured on day 1 after LPS dosing with or without prophylactic A1AT. Circle and square symbols indicate WT and KO mice, respectively (mean ± s.d., $n = 6$, 7 or 8 mice per group, one-way ANOVA with Tukey's multiple comparisons test, $^{**}P = 0.0085$, $^{***}P = 0.0002$ for cohort 1 versus 2 comparison and $P = 0.0004$ for cohort 2 versus 4 comparison, $^{****}P < 0.0001$, n.s. = not significant where $P = 0.8864$). **e**, The red ROC curve shows the ability of the breath signal from **d** to robustly differentiate between normal NE activity in WT mice and uninhibited NE activity in KO mice during inflammation. The blue ROC curve shows the loss of a discernable difference in the breath signal between WT and KO mice due to prophylactic A1AT treatment ($n = 7$ or 8 mice per group as in **d**).

protein was observed in lung homogenates from inoculated mice (Fig. 4c). Thus, inflammation onset and resolution were represented at the sampled time points. Breath signal 10 min after vABN dosing was measured at each time point and exhibited similar dynamics to NE protein levels (elevated at 8 h and 1 d, reduced by 4 d and back to baseline signal by 7 d; Fig. 4d). Repeated vABN dosing did not elevate breath signal in healthy controls. Receiver operating characteristic (ROC) curve analysis showed that inoculated mice can be identified with high sensitivity and specificity at 8 h and 1 d via breath analysis (Fig. 4e). Furthermore, the convergence of the healthy and diseased breath signals, as indicated by decreasing area under the ROC curve (AUROC) with time, was reflective of inflammation resolution.

For individuals with AATD, inflammatory insults such as respiratory infections are particularly damaging to the lungs due to the deficiency of the endogenous NE inhibitor, alpha-1 antitrypsin (A1AT). Dysregulated NE activity leads to alveolar damage (that is, emphysema). Weekly prophylactic A1AT treatment is administered to prevent emphysema, and lung function and density are currently monitored using forced expiratory volumes and computed tomography imaging, respectively[43]. Aside from these highly downstream readouts for NE-mediated lung damage, there are no pharmacodynamic biomarkers that can be used to optimize A1AT dosing to minimize troughs in NE inhibition[44]. Therefore, we assessed the utility of our engineered breath signal as a pharmacodynamic biomarker for A1AT treatment (Fig. 5a). Mice were administered prophylactic A1AT, followed by a lipopolysaccharide (LPS) challenge to induce neutrophil recruitment and a vABN breath test to assess NE inhibition (Fig. 5b). Three different experimental timelines—D-1, D-2 and D-3—corresponding to LPS challenge 1, 2 or 3 days, respectively, after A1AT dosing were implemented to observe changes to the breath signal with A1AT clearance from the lungs. On the day of the breath test, approximately 11.1%, 3.2% and 1.2% of the initial dose remained in the lungs for D-1, D-2 and D-3 cohorts, respectively (Fig. 5c), and, with the exception of the D-1 cohort, NE protein was elevated at generally comparable levels across all LPS-challenged mice (Fig. 5d). Lower NE protein levels in the D-1 cohort may be attributed to higher A1AT levels, which have been shown to suppress neutrophil recruitment[45]. As expected, the average breath signal in untreated, LPS-challenged controls was elevated, and the breath signals in the treated cohorts captured the diminishing capacity of a single prophylactic A1AT dose to inhibit NE activity over time (Fig. 5e). When the LPS challenge was given 1 or 2 days after A1AT dosing, the average breath signal was significantly lower than that of untreated, LPS-challenged controls ($P < 0.0001$ and $P = 0.0244$, respectively). By day 3 after A1AT administration, the dose no longer protected against NE activity, as indicated by the poor distinction between untreated, LPS-challenged controls and the D-3 cohort, as determined by breath signal ($P > 0.9999$). This result was further supported by the negative correlation between breath signal and A1AT in the lungs (Fig. 5f) and ROC curve analysis (Fig. 5g). Thus, vABNs can be used to directly assess A1AT

inhibition of pulmonary NE activity to characterize the duration of therapeutic efficacy and inform dosing frequency. While these studies verified that we could monitor A1AT activity in vivo, they were completed in wild-type (WT) mice with intact A1AT expression. Therefore, A1AT dosing in this context was supplementary to endogenous A1AT, and the therapeutic goal in these studies was the suppression of NE activity to the baseline levels observed in healthy controls rather than to the normal NE activity that is expected during acute inflammation.

To better recapitulate the goal of A1AT therapies, vABN breath tests were completed in genetically engineered mouse models of AATD with *Serpina1a - e* gene knockout (KO)[46]. We sought to determine if vABN breath tests could resolve normal NE activity in WT C57BL/6 mice and pathologic, elevated NE activity in KO mice during acute inflammation (Fig. 6a). With this capability, we could then assess the ability of A1AT therapies to normalize NE activity in AATD. To test this hypothesis, vABN breath tests were conducted in both WT and KO mice before and after an LPS challenge (Fig. 6b). WT and KO mice produced equivalent baseline breath signals (Fig. 6c). After LPS administration, KO mice had a significantly higher breath signal compared to WT mice (Fig. 6d, $P=0.0004$), demonstrating the ability of vABNs to identify pathologic NE activity (Fig. 6e). The average breath signal in A1AT-treated KO mice was significantly lower than that of untreated KO mice (Fig. 6d, $P=0.0085$) and indistinguishable from that of WT mice with acute inflammation (Fig. 6e). Thus, the breath signals reflected the normalization of NE activity by prophylactic A1AT treatment. Taken together, these results illustrate the utility of our vABN platform for assessing protease-modulating therapies.

## Conclusions

We have developed a modular approach for rapid, sensitive and non-invasive detection of aberrant pulmonary protease activity via a 10 min breath test. We produced volatile-releasing peptide substrates by covalent attachment of volatile reporters at the peptide C-terminus. Substrates were subsequently formulated onto PEG nanocarriers for intrapulmonary delivery in mouse models of lung infection and AATD, where we verified the feasibility of a protease-driven breath signal. Cumulatively, we demonstrated that engineered breath signals can be used to monitor lung protease activity despite differences in biological parameters (for example, sex, age and so on; Supplementary Table 2), which are potential confounding factors for endogenous biomarkers.

Breath tests are practical diagnostic tools due to the ease and non-invasive nature of breath sampling. Many commercial sampling devices and receptacles exist to streamline breath collection. Moreover, miniaturized gas analysis tools with ppt–ppb detection limits (for example, ion mobility spectrometers[47]) are now available to bring breath analysis to the point of care. The rate-limiting step in the translation of breath volatiles to clinical diagnostics is the identification of disease-specific breath biomarkers. Here, we illustrate that breath biomarkers can be engineered de novo by leveraging disease biology and stimulus-responsive nanomaterials. Using this bottom-up approach, we maximize SNR by tuning key parameters through vABN composition that otherwise cannot be controlled in endogenous breath biomarkers. Furthermore, by using VOC reporters that are absent in the body, diet and environment, we can minimize noise. Finally, the modular vABN structure enables sensing of different proteases by a simple exchange of the peptide substrate. Thus, through the integration of volatiles into nanomaterials, we can expand beyond the conventional optical readout for protease activity and develop new tools for non-invasive disease monitoring.

A caveat of the current vABNs includes the use of HFAs. While we did not observe in vivo toxicity, HFAs have not been used in humans and should be further characterized. Work is currently underway to incorporate classes of VOCs with known, minimal toxicity, which will also enable vABN multiplexing for disease-specific volatile signatures in breath. While single protease detection is useful for disease monitoring, single biomarkers suffer from poor disease specificity. Therefore, we predict that the measurement of multiple proteases using multiplexed vABNs can provide the needed specificity for disease detection, as we have previously demonstrated using urinary reporters[18,22,48].

## Online content

Any methods, additional references, Nature Research reporting summaries, source data, extended data, supplementary information, acknowledgements, peer review information; details of author contributions and competing interests; and statements of data and code availability are available at https://doi.org/10.1038/s41565-020-0723-4.

Received: 26 September 2019; Accepted: 2 June 2020;
Published online: 20 July 2020

## References

1. Pereira, J. et al. Breath analysis as a potential and non-invasive frontier in disease diagnosis: an overview. *Metabolites* **5**, 3–55 (2014).
2. Amann, A. et al. Analysis of exhaled breath for disease detection. *Annu. Rev. Anal. Chem.* **7**, 455–482 (2014).
3. van Oort, P. M. et al. The potential role of exhaled breath analysis in the diagnostic process of pneumonia—a systematic review. *J. Breath Res.* **12**, 024001 (2018).
4. Hanna, G. B., Boshier, P. R., Markar, S. R. & Romano, A. Accuracy and methodologic challenges of volatile organic compound-based exhaled breath tests for cancer diagnosis: a systematic review and meta-analysis. *JAMA Oncol.* **5**, e182815 (2019).
5. Gaude, E. et al. Targeted breath analysis: exogenous volatile organic compounds (EVOC) as metabolic pathway-specific probes. *J. Breath Res.* **13**, 032001 (2019).
6. Savarino, V., Vigneri, S. & Celle, G. The $^{13}$C urea breath test in the diagnosis of *Helicobacter pylori* infection. *Gut* **45**, 18–23 (1999).
7. Lock, J. et al. Interpretation of non-invasive breath tests using $^{13}$C-labeled substrates—a preliminary report with $^{13}$C-methacetin. *Eur. J. Med. Res.* **14**, 547–550 (2009).
8. Ghoshal, U. C. How to interpret hydrogen breath tests. *J. Neurogastroenterol. Motil.* **17**, 312–317 (2011).
9. Timmins, G. S. Stable isotope biomarker breath tests for human metabolic and infectious diseases: a review of recent patent literature. *Expert. Opin. Ther. Pat.* **26**, 1393–1398 (2016).
10. Lange, J. et al. Volatile organic compound based probe for induced volatolomics of cancers. *Angew. Chem. Int. Ed.* **58**, 17563–17566 (2019).
11. Raissy, H. H. et al. A proof of concept study to detect urease producing bacteria in lungs using aerosolized $^{13}$C-urea. *Pediatr. Allergy Immunol. Pulmonol.* **29**, 68–73 (2016).
12. Bishai, W. R. & Timmins, G. S. Potential for breath test diagnosis of urease positive pathogens in lung infections. *J. Breath Res.* **13**, 032002 (2019).
13. Aberle, D. R. et al. Reduced lung-cancer mortality with low-dose computed tomographic screening. *N. Engl. J. Med.* **365**, 395–409 (2011).
14. Fuchs, S. I. et al. Lung clearance index for monitoring early lung disease in alpha-1-antitrypsin deficiency. *Respir. Med.* 116, 93–99 (2016).
15. Lagier, J. et al. Current and past strategies for bacterial culture in clinical microbiology. *Clin. Microbiol. Rev.* **28**, 208–236 (2015).
16. Taggart, C. C., Greene, C. M., Carroll, T. P., O'Neill, S. J. & McElvaney, N. G. Elastolytic proteases: inflammation resolution and dysregulation in chronic infective lung disease. *Am. J. Respir. Crit. Care Med.* **171**, 1070–1076 (2005).
17. Houghton, A. M. et al. Neutrophil elastase–mediated degradation of IRS-1 accelerates lung tumor growth. *Nat. Med.* **16**, 219–223 (2010).
18. Kwong, G. A. et al. Mass-encoded synthetic biomarkers for multiplexed urinary monitoring of disease. *Nat. Biotechnol.* **31**, 63–70 (2013).
19. Kwon, E. J. & Dudani, J. S. Ultrasensitive tumour-penetrating nanosensors of protease activity. *Nat. Biomed. Eng.* **1**, 0054 (2017).
20. Buss, C. G., Dudani, J. S., Akana, R. T. K., Fleming, H. E. & Bhatia, S. N. Protease activity sensors noninvasively classify bacterial infections and antibiotic responses. *EBioMedicine* **38**, 248–256 (2018).
21. Loynachan, C. N. et al. Renal clearable catalytic gold nanoclusters for in vivo disease monitoring. *Nat. Nanotechnol.* **14**, 883–890 (2019).
22. Kirkpatrick, J. D. et al. Urinary detection of lung cancer in mice via noninvasive pulmonary protease profiling. *Sci. Transl. Med.* **12**, eaaw0262 (2020).
23. Pham, C. T. N. Neutrophil serine proteases: specific regulators of inflammation. *Nat. Rev. Immunol.* **6**, 541–550 (2006).

24. Rubenfeld, G. D. et al. Incidence and outcomes of acute lung injury. *N. Engl. J. Med.* **353**, 1685–1693 (2005).
25. Laurell, C.-B. & Eriksson, S. The electrophoretic α1-globulin pattern of serum in α1-antitrypsin deficiency. *Scandinav. J. Clin. Lab. Invest.* **15**, 132–140 (1963).
26. Kasperkiewicz, P., Poreba, M., Snipas, S. J., Parker, H. & Winterbourn, C. C. Design of ultrasensitive probes for human neutrophil elastase through hybrid combinatorial substrate library profiling. *Proc. Natl Acad. Sci. USA* **111**, 2518–2523 (2014).
27. Anderson, B. M. et al. Application of a chemical probe to detect neutrophil elastase activation during inflammatory bowel disease. *Sci. Rep.* **9**, 13295 (2019).
28. Patton, J. S. The lungs as a portal of entry for systemic drug delivery. *Proc. Am. Thorac. Soc.* **1**, 338–344 (2004).
29. Gursahani, H., Riggs-Sauthier, J., Pfeiffer, J. & Lechuga-Ballesteros, D. Absorption of polyethylene glycol (PEG) polymers: the effect of PEG size on permeability. *J. Pharm. Sci.* **98**, 2847–2856 (2009).
30. Pelfrêne, A., Cave, M. R., Wragg, J. & Douay, F. In vitro investigations of human bioaccessibility from reference materials using simulated lung fluids. *Int. J. Environ. Res. Public Health* **14**, 112 (2017).
31. Ng, A. W., Bidani, A. & Heming, T. A. Innate host defense of the lung: effects of lung-lining fluid pH. *Lung* **182**, 297–317 (2004).
32. Teeguarden, J. G., Bogdanffy, M. S., Covington, T. R., Tan, C. & Jarabek, A. M. A PBPK model for evaluating the impact of aldehyde dehydrogenase polymorphisms on comparative rat and human nasal tissue acetaldehyde dosimetry. *Inhal. Toxicol.* **20**, 375–390 (2008).
33. Chiu, W. A. et al. Physiologically based pharmacokinetic (PBPK) modeling of interstrain variability in trichloroethylene metabolism in the mouse. *Environ. Health Perspect.* **122**, 456–463 (2014).
34. Nong, A. et al. Physiologically based modeling of the inhalation pharmacokinetics of ethylbenzene in B6C3F1 mice. *J. Toxicol. Environ. Heal. Part A* **70**, 1838–1848 (2007).
35. Krishnan, K., Gargas, M. L., Fennell, T. R. & Andersen, M. E. A physiologically based description of ethylene oxide dosimetry in the rat. *Toxicol. Ind. Health* **8**, 121–140 (1992).
36. Reddy, M. B. et al. Inhalation dosimetry modeling with decamethylcyclopentasiloxane in rats and humans. *Toxicol. Sci.* **105**, 275–285 (2018).
37. Beauchamp, J. Real-time breath gas analysis for pharmacokinetics: monitoring exhaled breath by on-line proton-transfer-reaction mass spectrometry after ingestion of eucalyptol-containing capsules. *J. Breath Res.* **4**, 026006 (2010).
38. Stein, R. L. & Strimpler, A. M. Catalysis by human leukocyte elastase. Aminolysis of acyl-enzymes by amino acid amides and peptides. *Biochemistry* **26**, 2238–2242 (1987).
39. Hammond, P. D., Stutzenberger, F. & Butler, R. N. Use of a disposable syringe as a novel economic breath-collection chamber for mice. *Contemp. Top. Lab. Anim. Sci.* **37**, 70–71 (1998).
40. Santos, A. M. et al. Role of $^{13}$C-urea breath test in experimental model of *Helicobacter pylori* infection in mice. *Helicobacter* **16**, 320–326 (2011).
41. Polverino, E., Rosales-mayor, E., Dale, G. E. & Dembowsky, K. The role of neutrophil elastase inhibitors in lung diseases. *Chest* **152**, 249–262 (2017).
42. Dudani, J. S., Warren, A. D. & Bhatia, S. N. Harnessing protease activity to improve cancer care. *Annu. Rev. Cancer Biol.* **2**, 353–376 (2017).
43. Sandhaus, R. A. et al. Clinical practice guidelines: the diagnosis and management of alpha-1 antitrypsin deficiency in the adult. *J. COPD Found.* **3**, 668–682 (2016).
44. Campos, M. A. et al. The biological effects of double-dose alpha-1 antitrypsin augmentation therapy: a pilot study. *Am. J. Respir. Crit. Care Med.* **200**, 318–326 (2019).
45. Jonigk, D. et al. Anti-inflammatory and immunomodulatory properties of α1-antitrypsin without inhibition of elastase. *Proc. Natl Acad. Sci. USA* **110**, 15007–15012 (2013).
46. Borel, F. et al. Editing out five *Serpina1* paralogs to create a mouse model of genetic emphysema. *Proc. Natl Acad. Sci. USA* **115**, 2788–2793 (2018).
47. Shvartsburg, A. A. et al. Ultrafast differential ion mobility spectrometry at extreme electric fields in multichannel microchips. *Anal. Chem.* **81**, 6489–6495 (2009).
48. Dudani, J. S., Ibrahim, M., Kirkpatrick, J., Warren, A. D. & Bhatia, S. N. Classification of prostate cancer using a protease activity nanosensor library. *Proc. Natl Acad. Sci. USA* 115, 8954–8959 (2018).

## Methods

**vABN synthesis and characterization.** HFA-modified peptides were synthesized by CPC Scientific (>95% purity). Briefly, the peptide substrate, Ac-CKKK(Cy5)-PE G4-Nle(O-Bzl)-Met($O_2$)-Oic-Abu-OH, was synthesized on Fmoc-Abu-CTC resin via standard Fmoc solid phase peptide synthesis. The peptide was cleaved from the resin using 30% HFIP solvent in DCM solvent for 30 min and subsequently coupled to the HFA reporter using DIC/HOBt coupling reagents in DCM under stirring conditions at room temperature for 2 h. The finished product was deprotected in trifluoroacetic acid (TFA) for 2.5 h, precipitated and washed in chilled ether two times and dried under vacuum overnight. The crude peptide was then purified using reversed phase HPLC (RP-HPLC). For vABN synthesis, HFA-modified peptides were conjugated to 40 kDa maleimide-functionalized eight-arm PEG (Jenkem) overnight at room temperature in deionized water (2:1 molar ratio of peptide to maleimide groups). Excess peptides were removed using spin filters (Millipore, 10 kDa molecular weight cut-off), and completed vABNs were stored in deionized water at 4 °C. vABNs were visualized using TEM imaging. Samples were prepared by placing a 1 mg ml$^{-1}$ vABN solution onto a TEM grid, wicking away the solution and staining the sample with 2% uranyl acetate.

**Real-time vapour analysis.** A triple quadrupole mass spectrometer with 1 l min$^{-1}$ sampling rate and ppq to ppt detection limit[49] was used to quantify HFA reporter concentrations in the headspace of in vitro reactions and breath samples collected in glass vials during the in vivo experiments. Multiple reaction monitoring (MRM), in which both the $[M+H]^+$ precursor ions and the $[M–HF]^+$ product ions are monitored, was used for sensitive and selective detection of HFA reporters. Data was acquired using Analyst software.

**In vitro cleavage assays.** To investigate reporter release as a function of NE concentration, vABNs equivalent to 10 µM substrate were reacted with picomolar to nanomolar NE in a 400 µl final reaction volume in capped 6 ml glass vials. After reacting for 10 min on a shaker, vapour analysis of the reaction headspace was completed by opening the vials at the inlet of the triple quadrupole mass spectrometer. Protease specificity was subsequently assessed by reacting 10 µM vABN with 40 pM NE, proteinase 3 (PR3), granzyme B (GZMB), cathepsin B (CTSB), cathepsin D (CTSD), matrix metalloproteinase 9 (MMP9) or matrix metalloproteinase 13 (MMP13) and analysing the reporter signal in the headspace using the same method as before. For each protease, separate reaction vials were prepared for each time point separated by 5 min intervals to determine HFA reporter signal over time. To predict breath signal using the PBPK model, reporter release kinetics were further characterized for vABNs containing reporters HFA1, HFA3, HFA5 and HFA7. The $k_{cat}$ and $K_m$ for vABNs were derived by first determining the initial cleavage velocities ($v$) for different micromolar substrate concentrations reacted with a fixed 20 pM NE concentration, plotting the values in a Lineweaver–Burke plot and fitting a line to find the $x$ intercept ($-1/K_m$) and $y$ intercept ($1/v_{max}$). The $k_{cat}$ value was calculated by dividing $v_{max}$ by the NE concentration. All cleavage assays were completed in enzyme-specific buffers (NE, PR3, GZMB: 50 mM Tris, 300 mM NaCl, 0.05% (w/v) Brij-35, pH 7.5; CTSB: 25 mM MES, 2 mM DTT, 0.05% (w/v) Brij-35, pH 5.0; CTSD: 0.1 M sodium acetate, 0.2 M NaCl, 0.05% (w/v) Brij-35, pH 3.5; MMP9, MMP13: 50 mM Tris, 10 mM $CaCl_2$, 300 mM NaCl, 20 µM $ZnCl_2$, 1 mM $MgCl_2$, 0.05% (w/v) Brij-35, pH 7.5.)

**PBPK model.** For a complete description of the model, variables and equations, refer to the Supplementary Information.

**Partition coefficient studies.** Partition coefficients for HFA reporters were derived empirically to be used in the PBPK model. To determine the tissue:air partition coefficients ($H_{t:a}$) and blood:air partition coefficients ($H_{b:a}$) of HFA1, HFA3 and HFA5, blood in EDTA solution and lung tissue were first collected from female CD-1 mice and aliquoted into 20 ml volatile organic analysis (VOA) glass vials with rubber septa caps (Thermo Scientific). Then 5 µl of pure HFAs was vapourized inside separate VOA glass vials and 10 µl of vapourized HFA was transferred to empty reference vials and vials containing EDTA solution, blood or lung tissue using gas-tight syringes. Vials were then allowed to equilibrate for 4 h at 37 °C, after which, 10 µl of headspace from each vial was sampled using a gas-tight syringe, with the sample introduced into the triple quadrupole mass spectrometer. Partition coefficients were calculated using equations established by Gargas et al. (ref. [50]). For $H_{EDTA:a}$ and $H_{t:a}$: $(C_{ref}V_{vial} - C_i(V_{vial} - V_i))/(C_iV_i)$ where $C$ represents HFA concentration in the headspace, $V$ represents volume, and $i$ represents the compartment of interest (that is, EDTA or tissue). For the $H_{b:a}$: $((C_{ref}(V_{vial} - V_{EDTA}) - C_b(V_{vial} - V_{EDTA} - V_b) + (C_{ref} - C_b))H_{EDTA:a}V_{EDTA})/(C_bV_b)$.

**Lung infection models.** All animal studies were approved by the Massachusetts Institute of Technology's Committee on Animal Care and were completed in accordance with the National Institutes on Health Guide for the Care and Use of Laboratory Animals. For lung infection breath studies, 7- to 8-week-old female CD-1 mice (Charles River) were administered an inoculum of $1.5 \times 10^6$ c.f.u. *P. aeruginosa* (strain PA01) in 50 µl PBS buffer via intratracheal instillation. The inoculum was prepared by diluting an overnight culture 1:10–1:50 in LB media, allowing the secondary culture to grow to an optical density of ~0.5, washing the secondary culture twice with PBS and resuspending the bacteria in PBS. Total NE content in the lungs was quantified 4, 8, 12, 24 and 48 h after inoculation by running ELISA assays on lung homogenates (R&D Systems, Mouse Neutrophil Elastase/ELA2 DuoSet ELISA). Lung homogenates were prepared by collecting the lungs, placing lungs in gentleMACS C tubes containing 2 ml chilled cOmplete protease inhibitor cocktail (Roche) in PBS and homogenizing using a gentleMACS dissociator. Bacterial burden was quantified by plating 1:10–1:10,000 dilutions of lung homogenates on solid LB agar with overnight incubation and subsequent colony counting.

**Visualization of vABN and NE in lung tissue sections.** At 24 h after initiating lung infection in female CD-1 mice, 10 µM vABNs in 50 µl PBS was administered via intratracheal instillation. Mice were euthanized via isoflurane overdose 5–10 min after vABN administration. The lungs were immediately collected with the trachea, filled with 1 ml 1:1 optimal cutting temperature (OCT) embedding compound/PBS mixture, placed in an OCT-filled cryomould, snap frozen in liquid-nitrogen-chilled isopentane and stored at −80 °C. Lungs from healthy control mice were collected and embedded using the same methods for comparison of NE content. Frozen tissues were cut into 7-µm-thick sections using a cryostat and placed on Fisherbrand Superfrost Plus microscope slides. Immunofluorescence staining for NE was completed to visualize co-localization of NE and vABNs. Briefly, tissue sections were fixed in chilled acetone (−20 °C) for 10 min and rehydrated using three washes in PBS (5 min each). Slides were then blocked using PBS containing 1% bovine serum albumin (BSA) for 1 h at room temperature before overnight incubation with a 1:200 dilution of rabbit anti-mouse NE antibody (Abcam, ab68672) at 4 °C. After overnight incubation, slides were washed three times with PBS and incubated with a 1:1,000 dilution AlexaFluor 488-labelled goat anti-rabbit IgG secondary antibody for 1 h at room temperature (Thermo Fisher, A11034). Following three PBS washes, tissues were counterstained with Hoechst, washed three more times with PBS and mounted using ProLong Diamond Antifade Mountant. Slides were imaged using a Leica TCS SP8 confocal microscope.

**Breath collection and analysis.** For vABN breath tests, 10 µM vABNs in 50 ul PBS were administered into mice via intratracheal instillation. At 10 min after vABN administration (unless otherwise specified), mice were placed inside a breath collection apparatus consisting of a 100 ml syringe (Wilburn Medical) connected to a stopcock valve (Cole Parmer, UX-30600-05) with a 23G needle (BD, 305145)[39,40]. The syringe was sealed for 2 min to allow breath volatiles to accumulate in the syringe headspace. After 2 min, the valve was opened and 55 ml of headspace was displaced into five 12-ml Exetainers (Labco Limited) by puncturing the rubber septum with the needle and pushing the syringe plunger. To measure the HFA reporter signal in breath samples, Exetainers were uncapped at the inlet of a triple quadrupole mass spectrometer and analysed for 0.25 min each. Signal peaks were integrated to determine total counts and converted to ppb units.

**Infection-monitoring studies.** To model dynamic changes in NE activity during the onset and resolution of infection, CD-1 mice were treated with an antibiotic (10 mg kg$^{-1}$ ciprofloxacin via intraperitoneal injection) 24 h and 48 h after inoculation with PA01. vABN breath tests were completed at the baseline before inoculation and 8 h, 1 d, 2 d, 4 d and 7 d after inoculation. In a separate cohort, mice that were infected at the same time as those receiving the vABN breath tests were euthanized at the experimental time points for histology and quantification of NE in lung homogenates. Lung tissues for histology were paraffin embedded, and 5-µm-thick tissue sections were H&E stained and imaged using a slide scanner.

**A1AT augmentation studies.** A 1 mg prophylactic dose of human A1AT (Sigma Aldrich, A6150) was administered via intratracheal instillation into 8- to 10-week-old female C57BL/6N mice (Charles River). One, two or three days following A1AT dosing, 50 µg pure *Escherichia coli* LPS (Invivogen, tlrl-3pelps) in 50 µl PBS was administered via intratracheal instillation to induce acute lung inflammation. At 24 h after the LPS challenge, vABN breath tests were completed. NE and human A1AT in lung homogenates was quantified using an ELISA (Bethyl Laboratories, E88-122). Pearson's correlation coefficient, $r$, was calculated to assess the relationship between the breath signal and A1AT in the lungs across all time points.

**Breath studies in genetically engineered mouse models of AATD.** WT C57BL/6 mice and *Serpina1a - e* KO mice of C57BL/6 background[46] were a kind gift from the laboratory of Christian Mueller (U Mass). Experiments were conducted on male mice 27–30 weeks old. A single vABN breath test in this study consisted of administering 20 µM vABNs via intratracheal instillation and collecting a 2 min breath sample 10 min after vABN administration. To measure the reporter signal in breath samples, 15 ml of breath (3 ml drawn from each of the five Exetainers per mouse) was injected into the port of a proton transfer reaction–mass spectrometer (Ionicon PTR-TOF 1000Ultra). WT and *Serpina1a - e* KO mice were divided into the following experimental groups: LPS– (healthy controls), LPS+ and A1AT+LPS+ ($n$=7–8). At day −3, vABN breath tests were completed on experimental groups at the baseline (without any inflammatory stimuli in the

lungs). On day −1, A1AT+LPS+ mice were administered a 1 mg prophylactic dose of human A1AT in 50 µl PBS via intratracheal instillation. On day 0, mice were given 40 µg *Salmonella enterica* LPS (Sigma Aldrich, L2137) in 40 µl PBS via intratracheal instillation. At 24 h after LPS dosing, vABN breath tests were completed.

**Statistical analysis.** Ordinary one-way ANOVA with Tukey's multiple comparisons test, ROC curve analyses and calculations for Pearson's correlation coefficient were completed in GraphPad Prism 8.

**Reporting Summary.** Further information on research design is available in the Nature Research Reporting Summary linked to this article.

## Data availability

Research data is available online at https://doi.org/10.5281/zenodo.3840591. Source data are provided with this paper.

## Code availability

Code for the PBPK model is available online at https://github.com/NN19092108A/PBPKmodel. Source data are provided with this paper.

## References

49. Ong, T. et al. Use of mass spectrometric vapor analysis to improve canine explosive detection efficiency. *Anal. Chem.* **89**, 6482–6490 (2017).
50. Gargas, M. L., Burgess, R. J., Voisard, D. E., Cason, G. H. & Andersen, M. E. Partition coefficients of low-molecular-weight volatile chemicals in various liquids and tissues. *Toxicol. Appl. Pharmacol.* **98**, 87–99 (1989).

## Acknowledgements

We thank H. Fleming (MIT) for critical editing of the manuscript; H. Ko (MIT) for assistance with experiments; C. Buss (MIT), M. Zieger (U Mass), D. Kotton (BU) and A. Wilson (BU) for helpful discussion; Q. Smith (MIT) for assistance with confocal imaging; and E. Roche (MIT), J. Dudani and A. Bekdemir (MIT) for feedback on the PBPK model. We thank C. Mueller (U Mass) for providing us with AATD mouse models. We thank the Koch Institute's Robert A. Swanson (1969) Biotechnology Center for technical support, specifically the Hope Babette Tang (1983) Histology Facility, the Biopolymers & Proteomics Core Facility, and the Microscopy Core Facility. We also thank N. Watson at the Whitehead Institute W.M. Keck Microscopy Facility for her TEM imaging services. This study was supported in part by a Global Health Innovation Partnership (GHIP) grant from the Bill and Melinda Gates Foundation, Massachusetts General Hospital and the Ragon Institute; funding from Janssen Research and Development; and funding from the Kathy and Curt Marble Cancer Research Fund to S.N.B. L.W.C. acknowledges support from the National Institute of Health Pathway to Independence Award (K99 EB28311). M.N.A. thanks the National Science Foundation Graduate Research Fellowship Program for support. S.N.B. is a Howard Hughes Institute Investigator.

## Author contributions

L.W.C. and S.N.B. conceived the study with suggestions from R.R.K. L.W.C. synthesized and characterized the nanoparticle sensors. L.W.C. and T.-H.O. carried out in vitro experiments. M.N.A. built the multicompartment model for in silico predictions of breath signal output, extracted in vivo parameters for reporter partitioning and completed in silico experiments. L.W.C. and K.E.H. carried out in vivo experiments. L.W.C., M.N.A. and T.-H.O. analysed the data. L.W.C. wrote the paper with contributions from S.N.B. and M.N.A. and feedback from all authors.

## Competing interests

S.N.B., L.W.C., M.N.A. and R.R.K. are listed as inventors on patent applications related to the content of this work. S.N.B. holds equity in Glympse Bio and Impilo Therapeutics; is a director at Vertex; consults for Cristal, Maverick and Moderna; and receives sponsored research funding from Johnson and Johnson.

## Additional information

**Supplementary information** is available for this paper at https://doi.org/10.1038/s41565-020-0723-4.

**Correspondence and requests for materials** should be addressed to S.N.B.

**Peer review information** *Nature Nanotechnology* thanks Marcin Drag, Hossam Haick and the other, anonymous, reviewer(s) for their contribution to the peer review of this work.

**Reprints and permissions information** is available at www.nature.com/reprints.

nature research

Corresponding author(s): Bhatia, Sangeeta

Last updated by author(s): Apr 5, 2020

# Reporting Summary

Nature Research wishes to improve the reproducibility of the work that we publish. This form provides structure for consistency and transparency in reporting. For further information on Nature Research policies, see Authors & Referees and the Editorial Policy Checklist.

## Statistics

For all statistical analyses, confirm that the following items are present in the figure legend, table legend, main text, or Methods section.

| n/a | Confirmed | |
|---|---|---|
| ☐ | ☒ | The exact sample size (*n*) for each experimental group/condition, given as a discrete number and unit of measurement |
| ☐ | ☒ | A statement on whether measurements were taken from distinct samples or whether the same sample was measured repeatedly |
| ☐ | ☒ | The statistical test(s) used AND whether they are one- or two-sided<br>*Only common tests should be described solely by name; describe more complex techniques in the Methods section.* |
| ☐ | ☒ | A description of all covariates tested |
| ☐ | ☒ | A description of any assumptions or corrections, such as tests of normality and adjustment for multiple comparisons |
| ☐ | ☒ | A full description of the statistical parameters including central tendency (e.g. means) or other basic estimates (e.g. regression coefficient) AND variation (e.g. standard deviation) or associated estimates of uncertainty (e.g. confidence intervals) |
| ☐ | ☒ | For null hypothesis testing, the test statistic (e.g. *F*, *t*, *r*) with confidence intervals, effect sizes, degrees of freedom and *P* value noted<br>*Give P values as exact values whenever suitable.* |
| ☒ | ☐ | For Bayesian analysis, information on the choice of priors and Markov chain Monte Carlo settings |
| ☒ | ☐ | For hierarchical and complex designs, identification of the appropriate level for tests and full reporting of outcomes |
| ☐ | ☒ | Estimates of effect sizes (e.g. Cohen's *d*, Pearson's *r*), indicating how they were calculated |

*Our web collection on statistics for biologists contains articles on many of the points above.*

## Software and code

Policy information about availability of computer code

| | |
|---|---|
| Data collection | Analyst software was used for data acquisition on the mass spectrometer. Custom code was written in Matlab R2017a for in silico experiments. Leica Application Suite X (LAS X) was used for confocal microscope image acquisition. Tecan i-control software (Version 3.7.3.0) was used to collect data on a Tecan Infinite 200pro microplate reader (Tecan). |
| Data analysis | Microsoft Excel (Version 1908) and GraphPad Prism (Version 8.1.0) were used to analyze data. |

For manuscripts utilizing custom algorithms or software that are central to the research but not yet described in published literature, software must be made available to editors/reviewers. We strongly encourage code deposition in a community repository (e.g. GitHub). See the Nature Research guidelines for submitting code & software for further information.

## Data

Policy information about availability of data

All manuscripts must include a data availability statement. This statement should provide the following information, where applicable:

- Accession codes, unique identifiers, or web links for publicly available datasets
- A list of figures that have associated raw data
- A description of any restrictions on data availability

Data is available upon request.

# Field-specific reporting

Please select the one below that is the best fit for your research. If you are not sure, read the appropriate sections before making your selection.

☒ Life sciences ☐ Behavioural & social sciences ☐ Ecological, evolutionary & environmental sciences

For a reference copy of the document with all sections, see nature.com/documents/nr-reporting-summary-flat.pdf

# Life sciences study design

All studies must disclose on these points even when the disclosure is negative.

| | |
|---|---|
| Sample size | Sample size are provided in the figure legends for each experiment and were determined based on prior experience with effect size and consistency of differences between groups. |
| Data exclusions | No data was excluded for in vitro experiments. Pre-established exclusion criteria based on failed intratracheal injection was used for in vivo experiments; animals were excluded solely on the basis of these pre-established criteria. |
| Replication | All experiments were repeated independently at least twice with similar results. |
| Randomization | No randomization of mice was completed. For breath studies, groups were established before infection or LPS dosing. All mice were sex- and age-matched. |
| Blinding | For histological evaluation of toxicity, lung tissues were analyzed by a veterinary pathologist who was blinded to the treatment groups. For all other experiments, investigators were not blinded to the groups and treatments during experiments. Data reported are not subjective due to the quantitative assays used as described in the methods section. |

# Reporting for specific materials, systems and methods

We require information from authors about some types of materials, experimental systems and methods used in many studies. Here, indicate whether each material, system or method listed is relevant to your study. If you are not sure if a list item applies to your research, read the appropriate section before selecting a response.

## Materials & experimental systems

| n/a | Involved in the study |
|---|---|
| ☐ | ☒ Antibodies |
| ☒ | ☐ Eukaryotic cell lines |
| ☒ | ☐ Palaeontology |
| ☐ | ☒ Animals and other organisms |
| ☒ | ☐ Human research participants |
| ☒ | ☐ Clinical data |

## Methods

| n/a | Involved in the study |
|---|---|
| ☒ | ☐ ChIP-seq |
| ☒ | ☐ Flow cytometry |
| ☒ | ☐ MRI-based neuroimaging |

## Antibodies

| | |
|---|---|
| Antibodies used | Anti-neutrophil elastase antibody (Abcam, Cat. No. ab68672), AlexaFluor 488-labeled goat anti-rabbit IgG antibody (ThermoFisher, Cat. No. A11034) |
| Validation | The Abcam antibody was grown in rabbits and was verified by the vendor to react with mouse and human neutrophil elastase. The vendor has also tested the antibody for the following applications: immunocytochemistry/immunofluorescence, Western blots, and immunohistochemistry on frozen or paraffin-embedded tissue sections. The ThermoFisher antibody was characterized by the vendor. |

## Animals and other organisms

Policy information about studies involving animals; ARRIVE guidelines recommended for reporting animal research

| | |
|---|---|
| Laboratory animals | All animal studies were approved by the Massachusetts Institute of Technology (MIT) committee on animal care (MIT protocol 0619-034-22). Female CD-1 mice (7-8 week old, Charles River) were infected with Pseudomonas aeruginosa for breath studies and immunofluorescence staining for neutrophil elastase. Uninfected, female CD-1 mice (7-8 weeks old, Charles River) were used in toxicity studies. Female C57BL/6N mice (8-10 weeks old, Charles River) were administered A1AT and/or LPS for A1AT augmentation studies. Male C57BL/6 mice (wildtype and Serpina 1a-e knockouts, 27-30 weeks old, gift from the laboratory of Christian Mueller at the University of Massachusetts) were administered A1AT and/or LPS for breath studies. Complete descriptions can be found in the corresponding figure legends and Methods. |

| | |
|---|---|
| Wild animals | This study did not involve wild animals. |
| Field-collected samples | This study did not involve field-collected samples. |
| Ethics oversight | All animal studies were approved by the Massachusetts Institute of Technology (MIT) committee on animal care (MIT protocol 0619-034-22). All animals received human care, and all experiments were conducted in compliance with institutional and national guidelines. |

Note that full information on the approval of the study protocol must also be provided in the manuscript.